Adaptive Controller with PID, FOPID, and NPID Compensators for Tracking Control of Electric – Wind Vehicle

Mohamed A. Shamseldin [1*]
[1]Department of Mechanical Engineering, Faculty of Engineering and Technology, Future University in Egypt, Cairo, Egypt
Email: Mohamed.abelbbar@fue.edu.eg
*Corresponding Author

Abstract— **This paper presents a new combination between the Model Reference Adaptive Control (MRAC) with several types of PID's controllers (PID, Fractional order PID (FOPID), and Nonlinear PID (NPID)) optimized using a new Covid-19 algorithm. The proposed control techniques had been applied on a new model for an electric-wind vehicle, which can catch the wind that blows in the opposite direction of a moving vehicle to receive wind; a wind turbine is installed on the vehicle's front. The generator converts wind energy into electricity and stores it into a backup battery to switch it when the primary battery is empty. The simulation results prove that the new model of electric–wind vehicles will save power and allow the vehicle to continue moving while the other battery charges. In addition, a comparative study between different types of control algorithms had been developed and investigated to improve the vehicle dynamic response. The comparison shows that the MRAC with the NPID compensator can absorb the nonlinearity (air resistance and wheel friction) where it has a minimum overshoot, rise time, and settling time (35 seconds) among other control techniques compensators (PID and FOPID).**

Keywords—Electric Vehicle (EV); Adaptive Control; Covid-19; Wind Turbine.

I. INTRODUCTION

After 25 years of lead-acid battery production, Thomas Parker invented the first electric car in 1884. Several electric car replicas were designed after that period [1]. Due to advancements in internal combustion engine technology and lower mass manufacturing costs, the electric car sector has fallen behind [2]. Between 1970 and 1980, an energy crisis pushed electric vehicles back to the forefront [3]. In comparison to traditional cars, it currently lacks high and long speed ranges. As a result, adequate technical progress was not possible [4].

Many firms have created electric automobiles up till now. These vehicles, however, have a limited range and cannot go at high speeds. Longer-distance vehicles are now being manufactured because to advancements in electric motor and battery technology [5]. Despite the longer range of ranges, the time it takes to charge the battery is extremely long. As a result, electric vehicles have yet to reach their full potential. The influence of different gearboxes on energy usage has been explored by T. HOFMAN and C.H.DAI. The fixed gear system, manual gearbox, and CVT gearbox have all been used to explore the powertrain system [6] - [8].

Alternative energy vehicles, such as solar-powered, hybrid, and plug-in hybrid vehicles, are becoming increasingly popular. Electric automobiles are gradually displacing gasoline-powered vehicles. Internal combustion engines produce a great deal of pollution [9]. It is at this point that the necessity for entirely sustainable and pollution-free energy-powered cars emerges [10]. Wind energy is free, renewable, inexhaustible, and abundant in the atmosphere. China is the world's greatest wind energy generator, with 145,362 MW. A wind turbine is a device that uses mechanical energy to transform the kinetic energy of the wind into mechanical energy and electricity [11] - [13].

Electric automobiles are becoming more popular as a pollution-reduction alternative to fuel vehicles. Electric cars, on the other hand, have a disadvantage in terms of travel range [14]. An electric car's average trip distance is shorter than that of a fuel vehicle. Charging the batteries while the vehicle is in motion can extend the range of electrically propelled vehicles [15]. This can be accomplished by capturing air currents and using them as a source of energy.

There are two types of wind resistance that act as a vehicle moves: frictional drag and form drag. Frictional drag is caused by air viscosity, while form drag is caused by differences in air pressure in the front and rear of the vehicle. We can absorb energy from a stationary wind turbine positioned near a road when it rotates owing to the air produced by the movement of automobiles beside it [16] - [18].

If the wind streams can be captured within the vehicle, they can be used to recuperate some of the energy that has been consumed to overcome the vehicle's form drag. This device works by installing a wind turbine in front of a vehicle that rotates and converts the kinetic energy into electrical energy using a generator [12], [10].

The chamber has a front air intake entrance and a back air exit vent. Sound-absorbing materials eliminate the noise generated by the wind turbine [19], [8]. This energy is stored in a battery separate from the vehicle's battery system. This, in turn, works as a reservoir, increasing the vehicle's efficiency over time. The vehicle must be charged externally, much like a regular car, and it is later supported by wind energy [20]. The research's major goal is to conserve the planet, which is in grave danger due to many sorts of

pollution, primarily from growing and wide-ranging automobiles that emit emissions at a high rate [10], [11].

In the event of a rapid disruption or parameter modification, traditional control approaches are unable to provide the requisite speed tracking with high accuracy [21]. Therefore, the propulsion system has played a crucial role in determining how well an EV performs overall. The researchers concentrated on creating controls for the electric vehicle's propulsion system [22]-[26]. Two crucial parameters efficient performance and optimal energy management require thorough and targeted research. The controller should deliver the fastest possible speed while consuming the least amount of energy [26]-[31]. Due to the fluctuating road conditions, the EV with a wind turbine is very nonlinear, time-independent, and unreliable. As a result, it is difficult to build a controller that completely removes external disturbances and manages uncertainty with a little control signal [32]-[37].

Due to its simplicity and ease of tuning, traditional PID controllers are frequently utilized in a variety of industrial applications. However, they do not guarantee desired dynamic performance and do not operate efficiently under a variety of operating situations [38]-[40]. Advanced control techniques such as adaptive control, variable structure control, fuzzy control, and neural networks can be used to solve this challenge [41]. Although the variable structure controller is simple, it is challenging to put into practice [42], [43]. This is due to the risk of an abrupt shift in the control signal, which could cause the system to malfunction [44].

A neural network-based motor control system has a high ability to address the system's structure uncertainty and disturbance, but it takes more computer power and data storage space [45]. Even for uncertain nonlinear systems, fuzzy control theory usually provides nonlinear controllers capable of performing many sophisticated nonlinear control actions [46]. Unlike traditional control design, an FLC does not necessitate accurate knowledge of the system model, such as the system transfer function's poles and zeroes. Although a fuzzy-logic control system based on an expert knowledge database requires fewer calculations, it does not have enough capacity to handle the new rules [47] - [49].

Adaptive control is a common control strategy for developing advanced control systems with improved performance and accuracy [50], [51]. MRAC (model reference adaptive control) is a direct adaptive approach with some configurable controller settings and a way to adjust them. Adaptive controllers, as opposed to the well-known and simply structured fixed gain PID controllers, are much more successful at dealing with unknown parameter fluctuations [52], [53].

This paper presents a new strategy for charging the backup battery of EV through the vehicle motion by attached wind turbine enhanced with the nozzle to improve the generated power. Also, this study improves the dynamic response using adaptive controllers with different types of compensators. The first type of compensator is the PID control which has the advantage of simplicity and is easy to tune. The second type of compensator is the Fractional order PID (FOPID) which can deal with the nonlinear behavior of complex systems. The third type is the enhanced nonlinear PID (NPID) that its coefficients merged with nonlinear factors. The proposed control techniques parameters were obtained according to the new Covid-19 optimization technique. The COVID-19 optimization considers a highly effective technique to find the optimal value based on a multi-objective function.

The paper is organized as follows; the first section illustrates the electric vehicle with a wind-turbine recharger model. The second section demonstrates the proposed control techniques. The third section results of each control technique. The fourth section is the conclusion.

II. ELECTRIC VEHICLE WITH WIND TURBINE MODEL

This section illustrates the proposed system components of the Electric vehicle with the Wind Turbine Recharger model. The first subsection is the overview, the second subsection is the vehicle dynamics and the third subsection demonstrates the system parameters.

A. System Overview

As indicated in Fig. 1, a new technique for utilizing renewable energy sources such as wind turbines is to install them beneath the front bumper. When the car travels forward, it encounters air resistance. The air mass's resistance strikes turbine blades, causing power to be generated. The generated energy is stored in a battery before being used in the BLDC motor. As a result, less fuel is used to produce energy, lowering the cost.
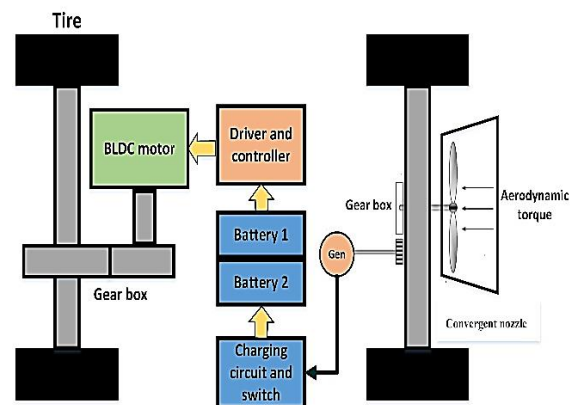

Fig. 1. Electric Vehicle with Wind Turbine Recharger schematic diagram.

Wind turbines generate electricity based on the speed of the wind and the diameter of the rotating blades. Wind speed increases by two times, resulting in an eightfold increase in power generation. As a result, by altering the fluid dynamic character of the wind at the blades, more power may be created than with a traditional wind turbine at the same wind speeds. Furthermore, power generation can begin at considerably lower wind speeds, expanding the number of potential wind power producing sites. A nozzle is a device that compensates for pressure to increase the velocity of a fluid as it exits an enclosed chamber. In the design below, the velocity of the wind at the outlet increases due to the convergent nozzle in Fig. 2, which increases the velocity of the wind attacking the wind turbine blades. As a result, the wind turbine spins quicker.
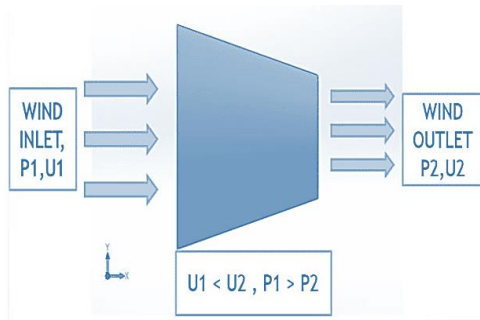
Fig. 2. Convergent nozzle.

Power, torque, and thrust are three indicators that fluctuate with wind speed and represent a wind turbine's performance. The rotor's power is determined by the quantity of energy it captures, the gearbox's torque is determined by the size of the gearbox, and the rotor thrust has a significant impact on the tower's structural design. A wind turbine turns the energy contained in moving air into electricity. The following equation shows how air density, power coefficient, air density, and turbine swept area effect the captured energy:

$$Power\ in\ the\ wind = \frac{1}{2}.\tau.\rho.A.U^3 \qquad (1)$$

Where ρ is air density (Kg/m^3), A is swept area of wind mill rotor (m^2), U is wind speed (m/s) and τ is power coefficient.

According to physicist Betz, the maximum power that can be obtained from an ideal turbine rotor with infinite blades from wind under perfect conditions is 59.26% (0.5926 times) of the power available in the wind. This limit is known as the Betz limit. Due to structural and economic concerns, wind turbines are designed with two or three blades, and the quantity of power they can generate is closer to 50 percent (0.5 times) of the available power. Tip speed ratio (TSR) of a wind turbine is defined as:

$$\lambda = (\Omega \times R)/U \qquad (2)$$

Where Ω presents the mechanical speed at the rotor shaft of the wind turbine (rad/s), R is the radius of the blade (m), U acts the velocity of the air (m/s). The TSR, and blade pitch angle β, are used to calculate the rotor power coefficient, denoted by τ. The rotor power coefficient can be calculated as:

$$\tau = (Extracted\ power)/(Power\ in\ wind) \qquad (3)$$

Equation 1 can be written as:

$$Pout = 0.5 \times \rho \times \tau \times A = \pi r^2(\lambda, \beta) \times U^3 \times A \qquad (4)$$

Variable-speed wind turbines are equipped with a pitch change mechanism (Pitch angle control) to adjust the blade pitch angle and obtain a better power coefficient profile because it controls its rotation speed. Wind turbine consists of the following subsystems. First subsystem is the rotor blades and hub. Second subsystem is the nacelle which contains shafts, gearbox, couplings, brake, and generator. Third subsystem is the electrical system such as switchgear, transformers, cables, and power converters. By adding the nozzle, the output power of turbine can be modified to become as following.

$$P_{out} = 0.5 \times \rho \times \tau(\lambda, \beta) \times (U \times * Nz)^3 A \qquad (5)$$

Where Nz is the nozzle factor which can enhance the output power of wind turbine.

B. Vehicle Resistance Forces

The fundamentals of vehicle design include physics fundamentals, particularly Newton's second law of motion. Newton's second law states that an object's acceleration is proportionate to the net force applied to it. As a result, when the net force exerted on an item is not zero, it accelerates. Several forces act on a vehicle, and according to Newton's second law, the net or resultant force regulates motion. The vehicle's propulsion unit generates the force required to propel the vehicle ahead. The propulsion unit's force aids the vehicle in overcoming the opposing forces of gravity, air resistance, and tire resistance as shown in Fig. 3.
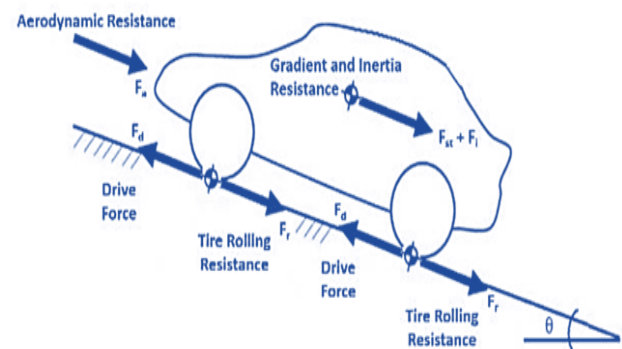

Fig. 3. Vehicle Resistance Forces.

This resistance force is called aerodynamic drag resistance. The aerodynamic drag resistance is calculated as follows;

$$f_a = 0.5\rho C_d A_f (v + v_0)^2 \qquad (6)$$

The aerodynamic resistance coefficient is determined experimentally according to vehicle shape as demonstrated in table I.

TABLE I. VEHICLE TYPE AND C_D

Vehicle type	C_d
Cabriole	0.5 – 0.7
Car	0.3 – 0.4
Bus	0.6 – 0.7
Truck	0.8 – 1.5
Optimal Design	0.2 – 0.3

Due to the elastic structure of the wheel, in front of the wheel contact center, a resistance force against the rotational movement of the tire occurs. The tire rolling resistance is calculated with this equality;

$$F_r = mgC_r \cos\theta \qquad (7)$$

Tire rolling resistance coefficient (C$_r$) varies according to the road surface and θ expresses the gradient of the path in degrees as shown in Table II.

The resistance of the vehicle moving on a sloping road. The gradient resistance appears due to the component of gravity.

$$F_{st} = mg\ sin\theta \tag{8}$$

TABLE II. ROAD SURFACE AND C_r

Road Surface	C_r
Concrete or Asphalt	0.013
Small Gravel Ground	0.02
Macadamized Road	0.025
Soil Road	0.1-0.35

According to the law of motion, during the acceleration and deceleration of an object, an inertial force is generated in the opposite direction to this motion. This force encountered during positive and negative acceleration of the vehicle is called inertia resistance. This resistance is calculated by this formula;

$$F_i = ma \tag{9}$$

Total resistance force

$$F_{load} = F_i + F_a + F_r + F_{st} \tag{10}$$

C. Electric Vehicle System Parameters

The proposed Electric vehicle system parameters can be summarized in Table III and Table IV.

TABLE III. ELECTRIC MOTOR PARAMETERS

No.	BLDC motor parameters		
1	Ra	0.1	The armature resistance (ohm)
2	Rf	0.1	The field resistance (ohm)
3	L_a	0.05	The armature inductance (Henrys)
4	L_f	0.005	The field inductance (Henrys)
5	K_b	0.2	Back EMF constant (Volt-sec/Rad)
6	K_t	0.2	Torque constant (Nm/A)
7	J_m	1	Rotor inertia (Kg.m2)
8	b_m	0.1	Mechanical damping (linear model of friction)
9	V	200	The rated voltage (V)

TABLE. IV. AUTOMOBILE AND ENVIRONMENTAL PARAMETERS

No.	Automobile and environmental parameters		
1	m	1600	Vehicle mass (Kg)
2	A	2.27	Vehicle Area (m)
3	C_d	0.28	Drag coefficient
4	n	3	Gear ratio
5	ζ	0.85	Efficiency of mechanical transmission
6	r	0.28	The tire radius (m)
7	μ	0.0083	Friction coefficient
8	ρ	1.5	Air density (Kg/m3)
9	α	0	Incline angle

The estimated parameters of the turbine which can produce power to charge the second backup battery of electric vehicle are demonstrated in table V. Also, a nozzle attached with turbine to enhance the generated power and achieve high efficiency.

TABLE. V. ESTIMATED TURBINE SPECIFICATIONS

No.	Particulars	Values
1	Hub diameter	140mm
2	Fan diameter	700mm
3	Number of blades	6
4	Blade thickness	3mm
5	Blade length	300mm
6	Blade width	25mm-55mm (taper)
7	Material	PVC
8	Nozzle factor (Nz)	2

By considering Coefficient of performance, Cp= 0.40 (For this wind turbine), Velocity of wind, U = 5.5 m/s, Density of air, ρ = 1.5 kg/m3, Radius of the turbine, r = 0.35 m. The front area and power of the turbine are found to be 0.384 m2. The following result shown in table 6 is obtained by simulating the model at various speeds of wind cars. The power generated by the turbine with respect to RPM and linear velocity is determined. Also, the test has been implemented with and without the nozzle to obvious the output power of two cases as shown in Fig. 4.
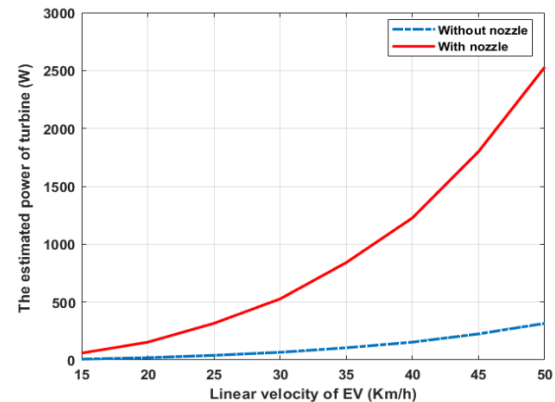

Fig. 4. The estimated output power versus linear speed of EV with and without the nozzle.

It can be noted that wind power generation depends on the velocity of the wind and the diameter of the rotating blades. If the speed of the wind increases by two times (using nozzle), then the power generation increases by eight times. Thus if increased the velocity of wind at the blades by modifying the fluid dynamic nature, more power can be generated compared to the conventional wind turbine at the same wind speeds as shown in Fig. 5.

III. MODEL REFERENCE ADAPTIVE CONTROL (MRAC)

A high-ranking adaptive controller is the Model Reference Adaptive Control (MRAC). It can be thought of as an adaptive servo system in which the required performance is described in terms of a reference model, which produces the desired command signal response. This is a quick and easy approach to describe a servo problem.

A. MRAC Based on Lyapunov Theory

A typical MRAC controller consists of a reference model, a control law, and an adaptive mechanism that updates the controller parameters based on the reference model and actual plant feedback error. The main premise of this adaptive controller is to construct a reference model that describes the controller's desired output, and then the adaptation law modifies the plant's unknown parameters until the tracking error converges to zero.

If there exists a function $V: R^n \rightarrow R$ that is the definite such that its derivatives along the solution of x=f(x) is negative semi-definite, then the solution x(t)=0 to x=f(x) is stable. If dv/dt is negative definite, the solution is asymptotically stable, V is called the Lyapunov function for the system $x = \dot{f}(x)$, moreover if $\frac{dV}{dt} < 0$ and V(x) → ∞ as $\|x\| \rightarrow \infty$, the solution is globally asymptotically stable. The

design steps can be divided to three steps. The first step is the derivation of the error equation where this differential equation of the error signal or states errors. The error equation should be written as a known transfer function controlled by a nonlinear input term. Usually, the linear part contains the reference model transfer function. The second step is a Lyapunov function is chosen as a function of the signal error and parameters errors. the third step is the time derivative of the Lyapunov function is calculated. the adaptive law is canceled such that $\dot{V}$ is negative definite or negative semi-definite. As an example assume the behavior of the EV system can be summarized to the first-order system that has the following transfer function.

$$y_P = \frac{b}{s+1}u \tag{11}$$

Where u is the controller output, y_P is the system iutput and b is system coeffeicient gain.

Also, the selected model reference can be as the following transfer function.

$$y_m = \frac{1}{s+1}r \tag{12}$$

Where y_m is the model reference output and r is the setpoint of the system.

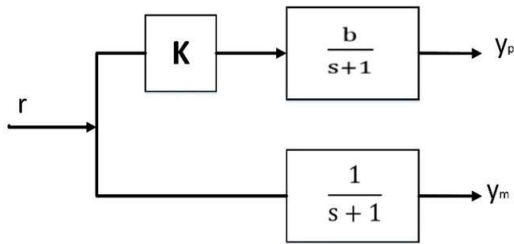The two systems can be rearranged as illustrated in Fig. 5.

Fig. 5. The basic construction of model reference adaptive control.

Required to adjust K such that $y_p \rightarrow y_m$.

$$e = y_P - y_n = (kb-1)\frac{1}{s+1}r \tag{13}$$

$$v = \frac{1}{2}e^2 + \frac{1}{2\gamma}(kb-1)^2 \tag{14}$$

$$\dot{V} = e\dot{e} + \frac{1}{\gamma}(Kb-1)b\dot{k} \tag{15}$$

$$\dot{V} = -e^2 + e(Kb-1)r + \frac{1}{\gamma'}(Kb-1)\dot{k} \tag{16}$$

$$\dot{V} = -e^2 + e(Kb-1)r + \frac{1}{\gamma'}(Kb-1)\dot{K} \tag{17}$$

$$e(Kb-1)r + \frac{1}{\gamma'}(Kb-1)\dot{K} = 0 \tag{18}$$

$$\dot{k} = -\gamma'e\,r \tag{19}$$

$$\dot{y} = -ay + bu \tag{20}$$

$$\dot{y_m} = -a_m y_m + b_m u_c \tag{21}$$

$$u = t_0 u_c - s_0 y \tag{22}$$

$$\dot{e} = \dot{y} - \dot{y_m} = -ay + b(t_0 u_c - s_0 y) + a_m y_m - b_m u_c \tag{23}$$

$$\dot{e} = -a_m(y-y_m) + (a_m - a - bs_0)y + (bt_0 - b_m)u_c \tag{24}$$

$$\dot{e} = -a_m e + (a_m - a - bs_0)y + (bt_0 - b_m)u_c \tag{25}$$

$$V = \frac{1}{2}e^2 + \frac{1}{2b\gamma}[(a_m - a - bs_0)^2 + (bt_0 - b_m)^2] \tag{26}$$

$$\dot{V} = e\dot{e} + \frac{1}{b\gamma}[(a_m - a - bs_0)(-b)\dot{s_0} + (bt_0 - b_m)bt\dot{_0}] \tag{27}$$

Substitute for $\dot{e}$ using

$$\dot{V} = e\dot{e} + \frac{1}{b\gamma}[(a_m - a - bs_0)(-b)\dot{s_0} + (bt_0 - b_m)bt\dot{_0}] \tag{27}$$

$$\dot{e} = -a_m e + (a_m - a - bs_0)y + (bt_0 - b_m)u_c \tag{28}$$

$$\dot{V} = -a_m e^2 + (a_m - a - bs_0)ye - \frac{1}{\gamma}(a_m - a - bs_0)\dot{s_0} + (bt_0 - b_m)u_c e + \frac{1}{\gamma}(bt_0 - b_m)\dot{t_0} \tag{29}$$

Choose $\dot{s_0} = \gamma ye$ and

$$\dot{t_0} = -\gamma u_c e \tag{30}$$

Then

$$\dot{V} = -a_m e^2 \tag{31}$$

B. MRAC with PID/FOPID/NPID Compensator

MRAC is designed to eliminate the difference between the output of the reference model and the actual speed. It does not take into account the error between reference speed and actual speed. This will cause high overshooting and high settling time. This disadvantage can be alleviated by adopting different types of compensators as displayed in Fig. 6. The first is a simple PID compensator. The second is the fractional order PID (FOPID) compensator. The third is the Nonlinear PID compensator (NPID).
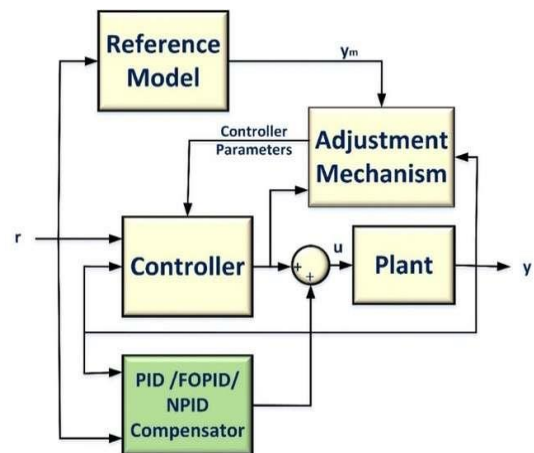

Fig. 6. Block diagram of MRAC with PID/ FOPID/NPID compensator.

The input of PID/FOPID/NPID compensators is the error between reference speed and actual speed. In this case, the controller action depends on both the MRAC and the PID/FOPID /NPID compensator as shown in Equation (32). This technique considers a new technique in this paper.

$$u = u_{MRAC} + u_{\underset{\overline{\underset{\overline{NPID}}{FOPID}}}{PID} \, compensator} \tag{32}$$

The transfer function of the PID controller is $K(s) = K_P + \frac{K_i}{s} + K_d s$. Where $K_p, K_i, \ k_d$ are proportional, integral and differential gains respectively. The most common form of a fractional order PID controller is the $PI^\lambda D^\mu$, including an integrator of order λ and a differentiator of order μ. where μ and λ can be any real numbers. The controller transfer function has the following form.

$$G_c = \frac{U(s)}{E(s)} = k_p + k_i \frac{1}{s^\lambda} + k_d s^\mu, (\lambda, \mu > 0) \tag{33}$$

The proposed form of NPID control can be described as follows.

$$u(t) = K_p[K_{n1}(e). e(t)] + K_i \int_0^t [K_{n2}(e). e(t)] \, dt$$
$$+ K_d \left[K_{n3}(e). \frac{de(t)}{dt} \right] \tag{34}$$

Where $K_{n1}(e), K_{n2}(e)$ and $K_{n3}(e)$ are nonlinear gains. The nonlinear gains represent any general nonlinear function of the error e which is bounded in the sector $0 < K_n(e) < K_n(e)$max.

There is a wide range of choices available for the nonlinear gain $K_n(e)$. One simple form of the nonlinear gain function can be described as.

$$K_{ni}(e) = ch(w_i e) = \frac{\exp(w_i e) + \exp(-w_i e)}{2} \tag{35}$$

Where $i = 1, 2, 3$.

$$e = \begin{cases} e & |e| \le e_{max} \\ e_{max} sgn(e) & |e| > e_{max} \end{cases} \tag{36}$$

where w_i and e_{max} are user-defined positive constants. The nonlinear gain $K_n(e)$ is lower bounded by $K_n(e)$min = 1 when e = 0, and upper-bounded by $K_n(e)$max = ch($w_i \, e_{max}$). Therefore, e_{max} stand for the range of deviation, and w_i describes the rate of variation of $K_n(e)$.

There are many methods to select the PID/FOPID/NPID compensator parameters such as trial and error and the Ziegler-Nichols rule [37], [38], [39]. In this research, the parameters of PID/FOPID/NPID compensator are selected simultaneously with the MRAC parameters (adaptation rate and model reference coefficients) based on a new Covid-19 optimization technique.

C. Covid-19 optimization

To deal with optimization difficulties, there are numerous bioinspired metaheuristics. Despite the fact that Covid-19 can be used to solve any sort of optimization problem, the focus of this section was on the optimization algorithms used to discover the best value for the PID controller parameters.

The initial population generation is the first step. One individual vector exists in the initial population (zero patient). It recognizes the first human infected, just like in the coronavirus epidemic scenario [54], [55].

In the second step, disease dissemination is determined by the actions of a single vector (zero patient), and numerous scenarios can be evaluated. In the first situation, some of the infected people die. According to the Covid-19 virus fatality rate, death is a possibility. Individuals who have been infected by them can no longer infect others. Individuals who survive the Covid-19 virus will infect new people in the second case (intensification). As a result, according to a particular probability, two types of disease transmission are evaluated. For use with standard spreaders. Infected individuals will infect new ones according to the rate of spreading rate, whereas infected individuals will infect new ones according to the coronavirus super spreading rate if the coronavirus spreading rate is high. Ordinary people and super-spreaders can both follow and find solutions in different ways. As a result, individuals are more likely to travel, allowing them to disseminate the sickness to potential alternative solutions [56], [57].

The third step is population modernization. For each generation, three populations are preserved and updated. The population is depleted. If a person dies, their body is added to this population and cannot be utilized again. The population has recovered. Infected people are sent to the recovered population after each repetition (after propagating the coronavirus according to the preceding stage). It is well known that there is a chance of reinfection. As a result, an individual who fits this demographic could be re-infected at any iteration as long as the reinfection requirement is met.

Individuals can be isolated when modeling social distancing methods, hence another condition must be measured. When an isolated person meets an isolation probability, it is assumed that they are moved to the recovered population as well. A newly contaminated population was discovered recently. According to the approach outlined in the previous phases, this population collects all sick individuals at each iteration. It's probable that during each repetition, newly infected individuals are born and, as a result, the virus spreads. Before the following iteration begins, it is recommended that such repeat individuals be removed from the population. The vaccines take into account the goal function that is employed to treat the sick population [58]-[60].

The stop criterion is the fourth stage. One of the most essential characteristics of the proposed method is its ability to terminate without the use of any parameters. This predicament arises because the recovered and deceased populations continue to grow over time, while the newly afflicted population is unable to infect new people. The number of infected people is thought to increase after a specific number of iterations. However, because recovered and dead populations are too large, and the size of the infected population decays over time, the newly infected population will be smaller than the present one after a certain iteration.

The higher and lower values of the PID controller parameters are included in the initial population of each

control technique. The performance of each row will be investigated according to the objective function in equation (37). The poor performance specifies the infected population, which has the possibility to die. While the good performance indicates the recovered population from corona antivirus.

$$J_t = (U_1 + U_2 + U_3 + U_4)/4 \qquad (37)$$

$$U_1 = \frac{|t_r - t_{rd}|}{t_{rd}}, \quad U_2 = \frac{|t_s - t_{sd}|}{t_{sd}},$$

$$U_3 = \frac{|e_{ss} - e_{ssd}|}{e_{ssd}}, \quad \text{and} \quad U_4 = \frac{|OS - OS_d|}{OS_d} \qquad (38)$$

Where (trd) is the desired rise time and (tr) is the measured rise time, (OSd) is the desired maximum overshoot and (OS) is the actual overshoot, (tsd) is the desired settling time and (ts) is the determining settling time, and (essd) is the desired steady-state error and (ess) is the estimated steady-state error.

It should be noticed that the goal function employs four sub-objective functions to try to satisfy the designer. The first sub-objective function focuses on reducing overall drive system rise time. The second sub-objective function is to shorten the time it takes for everything to settle down. The steady-state error is measured by the third sub-objective function. The needed overshoot is investigated in the fourth sub-objective function. Each sub-objective function has a value ranging from zero to one. As a result, the overall objective function takes into account the average of four sub-objective functions. The first step investigates the Probability of travel If Pt = 0 then the type of spreading is SR = (0 to 0.5). In case of Pt = 1 then the type of spreading SRR = (0.5 to 1). In the second step, the zero infected patient If Pt = 0 will become as follows.

$$X_{F0} = L_X + (U_X - L_X)S_R \qquad (39)$$

If zero infected patient If $Pt = 1$.

$$X_{F0} = L_X + (U_X - L_X)S_{RR} \qquad (40)$$

The third step investigates if Jt > PDIE then this patient is dead and generates a newly infected patient. In the case of Jt < PDIE then the newly infected patient will be as follows.

$$X_{new} = X_{old} \pm X_{old} \begin{bmatrix} U_1 D_R \\ (0.5U_2 + 0.5U_3)D_R \\ U_4 D_R \end{bmatrix} \qquad (41)$$

The optimization will be stopped if (Xnew = Xold) where the newly infected populations cannot infect new individuals. If the number of iterations ended before this previous condition. the COVID-19 cannot give the optimal solution. Therefore, to obtain the optimal parameters of the proposed controller must be (Xnew = Xold) to guarantee the global solution. Table VI demonstrates the used COVID-19 parameters through offline optimization. Fig.7 demonstrate the main steps of COVID-19 optimization technique.

TABLE. VI. THE COVID-19 PARAMETERS

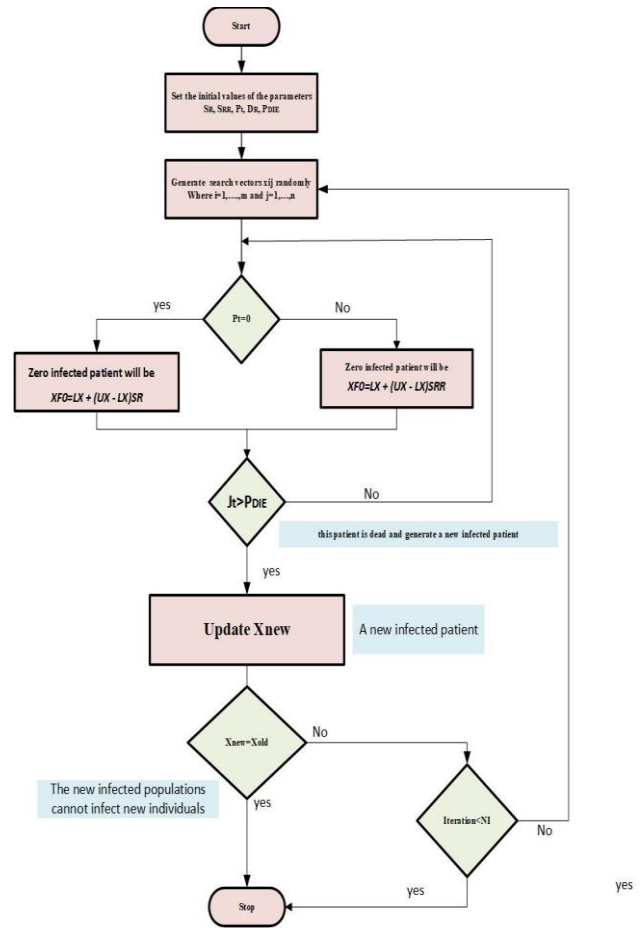| No.	COVID-19 Parameters	Symbol	Value
1	Probability of Death	PDIE	random value from 0 to 1
2	Death Rate	DR	random value from 0 to 1
3	Spreading Rate	SR	random value from 0 to 0.5
4	Super Spreading Rate	SRR	random value from 0.5 to 1
5	Probability of travel	Pt	random binary value 0 or 1

Fig. 7. COVID-19 optimization flowchart

IV. SIMULATION RESULTS

After the text edit has been completed, the paper is ready for the template. Duplicate the template file by using the Save As command, and use the naming convention prescribed by your conference for the name of your paper. In this newly created file, highlight all of the contents and import your prepared text file. You are now ready to style your paper; use the scroll down window on the left of the MS Word Formatting toolbar.

This section exhibits the EV performance using different types of control techniques. Three tests will be implemented: in the first test, the driver adjusts the EV at a fixed reference speed while in the second test the driver will change the reference speed continuously, the third test is applying the New European Driving Cycle (NEDC), it was understood that vehicle speed reference and cycle speed were the same.

Fig. 8 shows the EV linear velocity dynamic response at a fixed operating speed point. The objective is investigation the performance of the EV with wind turbine by applying several control techniques. It can be noted that the MRAC with NPID compensator has a faster response, smooth behavior, no overshoot, and zero steady-state error. The EV with wind turbine can reach the required speed in 35 seconds. In contrast to that, the other control techniques (PID, MRAC, MRAC with PID/FOPID compensator) have a slow response and high steady-state error. This means that the NPID compensator is more effective when combined with the

model reference adaptive control where it eliminates the overshoot without occurring slowing the system. Also, it deals with the nonlinearity of aerodynamics which exists in the EV with the wind turbine.
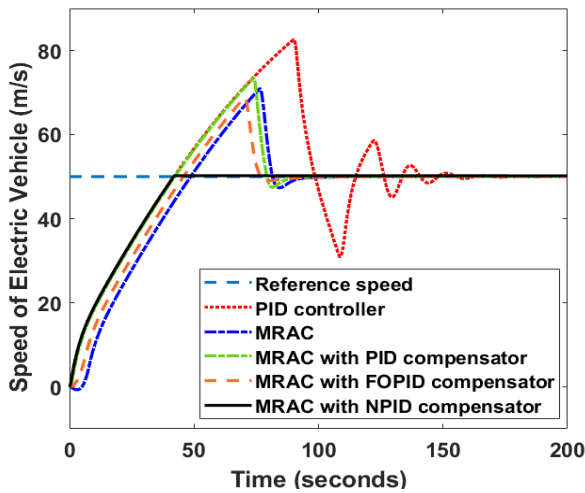

Fig. 8. The EV velocity response at fixed reference speed.

The controller output through the fixed operating point test is demonstrated in Fig. 9. It is clear that the controller output increases rapidly to reach the maximum value (200 V) and then stabilizes a period of time which differences from control technique to other. The steady state value is the same for all control techniques.
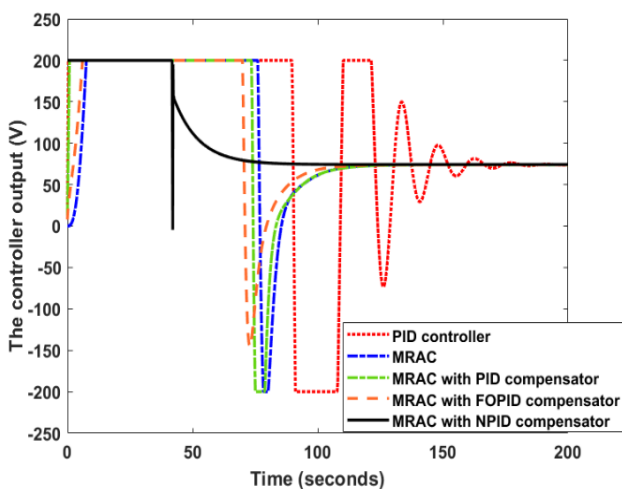

Fig. 9. The EV controller output at fixed reference speed.

The second test is used many operating points for reference speed to ensure the effectiveness of each control technique. Usually, the driver needs to change the reference speed of EV by traveling inside the city. So, this test simulates the behavior of EV inside the city. The profile of reference speed has the stairs form. It can be noted the MRAC with NPID compensators can track accurately the reference speed profile. The EV dynamic performance has no overshoot and a small rise time and settling time in case of the MRAC with NPID compensator compared to other control technique as demonstrated as Fig. 10.
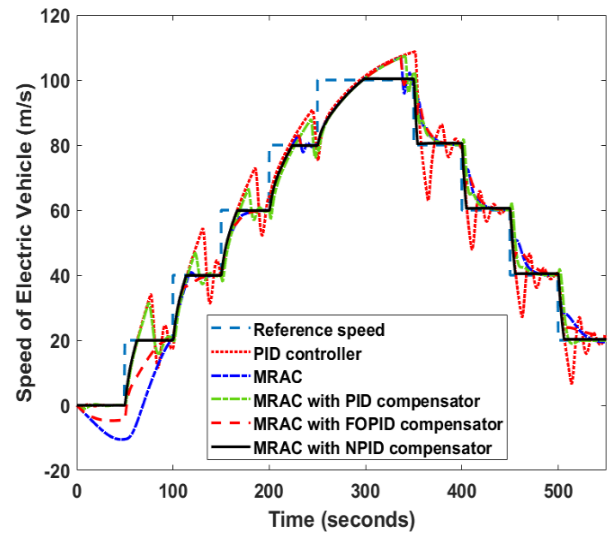

Fig. 10. The EV velocity response at variable reference speed.

Fig. 11. Illustrates the corresponding controller output of each control technique at several commands of reference speed. It is obvious that the rotor current fluctuates due to the continuous change in reference speed. Also, there is a shuttering in current at each new operating point especially in the MRAC with NPID compensator to can track rapidly the reference speed profile at satisfied dynamic response.
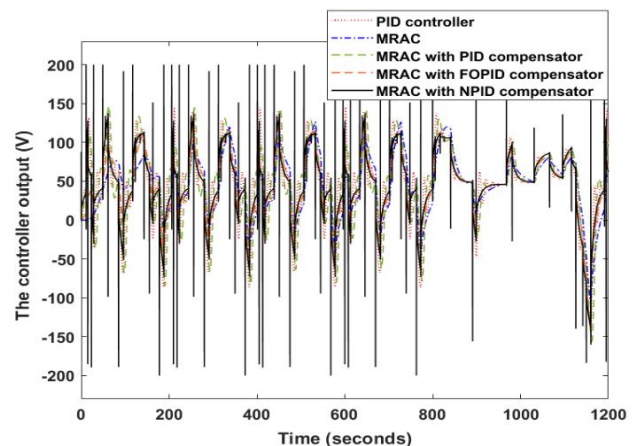

Fig. 11. The EV controller output at variable reference speed.

Various forms of standardized driving cycles are utilized all around the world. In the third test, the According to the simulation results including NEDC cycle, it was understood that vehicle speed and cycle speed were the same in case of the MRAC with NPID compensator. At this point, it is concluded that the energy consumption data obtained from the model is also correct. Simulation graph of NEDC cycle was created as demonstrated in Fig. 12.

Fig. 13 illustrates the corresponding rotor current of motor at NEDC cycle. It can be noted that the current fluctuates continuously according to NEDC cycle for each control technique. Also, it is clear that the peak of current in case of the MRAC with NPID compensator is small compared to other control techniques through this test.
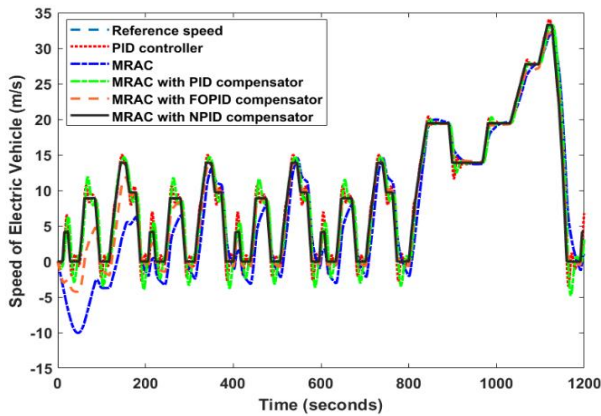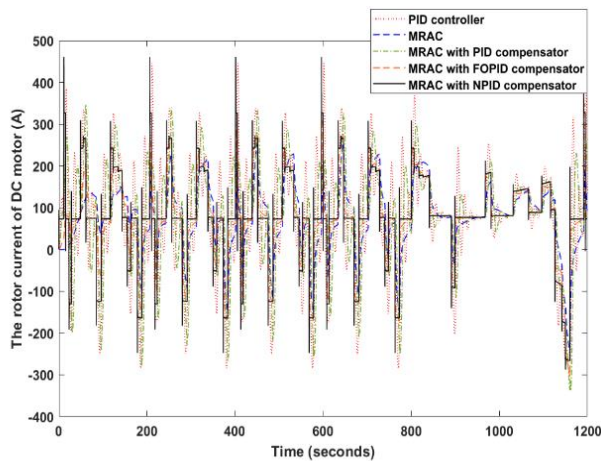
Fig. 12. The NEDC cycle with vehicle speed.

Fig. 13. The NEDC cycle with vehicle speed.

V. CONCLUSION

A new strategy to capture the wind energy through traveling the vehicle was presented. Also, a comparative study of different types of compensators (PID, FOPID and NPID) with adaptive controller to enhance the dynamic response of EV. A complete simulation for the proposed model was implemented and validated. A high overshoot and long settling time appears in case of the traditional controllers such as PID and adaptive controller. So, this paper investigated several types of compensators with the adaptive controller to treat this problem. The Covid-19 optimization algorithm was used to find the optimal values of proposed controllers' parameters. Many tests were executed to ensure the validity of each control technique. The first test is applying a fixed reference speed while the second and third tests use different operating points of reference speed. The results show the ability of the MRAC with NPID controller to absorb the high overshoot and reducing the rise and settling time compared to other techniques. Future work: Executing the proposed system practically. Also, use the solar energy to enhance the battery charge with wind turbine.

REFERENCES

[1] A. O. Kıyaklı and H. Solmaz, "Modeling of an Electric Vehicle with MATLAB/Simulink," Int. J. Automot. Sci. Technol., vol. 2, no. 4, pp. 9–15, 2018, doi: 10.30939/ijastech.475477.

[2] G. Wang, Y. Ji, L. Ren, H. Leng, and Y. Huang, "Performance analysis of a newly designed single air spring running gear for automated people mover (APM)," Veh. Syst. Dyn., vol. 59, no. 12, pp. 1963–1986, 2021, doi: 10.1080/00423114.2020.1798475.

[3] S. S. Salins, A. A. Khan, K. Riyaz, I. Mahmoud, S. Naeem, and K. H. Sachidananda, "Fabrication and working of a compressed air vehicle," J. Eur. des Syst. Autom., vol. 54, no. 1, pp. 97–103, 2021, doi: 10.18280/jesa.540111.

[4] J. Niu, Y. Wang, F. Liu, and R. Li, "Numerical study on comparison of detailed flow field and aerodynamic performance of bogies of stationary train and moving train," Veh. Syst. Dyn., vol. 59, no. 12, 2021, doi: 10.1080/00423114.2020.1794015.

[5] F. N. Morgin Carlos, B. M. Fotso, R. C. Talawo, and M. Fogue, "Aerodynamic Analysis of an Electric Vehicle Equipped With Horizontal Axis Savonius Wind Turbines," Int. J. Recent Trends Eng. Res., vol. 5, no. 6, pp. 17–26, 2019, doi: 10.23883/ijrter.2019.5057.lkaxl.

[6] Z. Chen, "Relationship between track stiffness and dynamic performance of vehicle–track–bridge system," Veh. Syst. Dyn., pp. 1–19, 2020, doi: 10.1080/00423114.2020.1792942.

[7] Y. Zhu, M. Feng, X. Wang, and X. Xu, "Research on intelligent vehicle autonomous overtaking based on single neuron pid control," in Proceeding of IEEE CCIS2012, 2012, pp. 2–5.

[8] A. Dinc and M. Otkur, "Optimization of Electric Vehicle Battery Size and Reduction Ratio Using Genetic Algorithm," in 2020 11th International Conference on Mechanical and Aerospace Engineering, 2020, pp. 281–285, doi: 10.1109/icmae50897.2020.9178899.

[9] M. F. Hossain and N. Fara, "Integration of wind into running vehicles to meet its total energy demand," Energy, Ecol. Environ., vol. 2, no. 1, pp. 35–48, 2017, doi: 10.1007/s40974-016-0048-1.

[10] M. R. Awal, M. Jusoh, M. N. Sakib, F. S. Hossain, M. R. Che Beson, and S. A. Aljunid, "Design and implementation of Vehicle Mounted Wind Turbine," ARPN J. Eng. Appl. Sci., vol. 10, no. 19, pp. 8699–8706, 2015.

[11] Z.-J. Guo and X.-Y. Kang, "Modeling and Analysis of Vehicle with Wind-solar Photovoltaic Hybrid Generating System," in 4th International Conference on Sustainable Energy and Environmental Engineering, 2016, pp. 566–570, doi: 10.2991/icseee-15.2016.95.

[12] S. P. Venkatesan, J. K. Soni, and A. Burugpalli, "Increasing efficiency of a wind turbine using a convergent nozzle in combination with a flanged diffuser," Int. J. Appl. Eng. Res., vol. 10, no. 11, pp. 10234–10240, 2015.

[13] Y. Cao, X. Li, G. Wu, X. Chen, and X. Tian, "Design and optimization of vertical axis wind turbine," Appl. Mech. Mater., vol. 150, pp. 148–153, 2012, doi: 10.4028/www.scientific.net/AMM.150.148.

[14] M. Shamseldin, M. A. Ghany, and Y. Hendawey, "Optimal Nonlinear PID Speed Control Based on Harmony Search for An Electric Vehicle Optimal Nonlinear PID Speed Control Based on Harmony Search for An Electric," Futur. Eng. J., vol. 2, no. 1, 2021.

[15] A. Gaurav and A. Gaur, "Modelling of Hybrid Electric Vehicle Charger and Study the Simulation Results," in 2020 International Conference on Emerging Frontiers in Electrical and Electronic Technologies (ICEFEET), 2020, pp. 1–6, doi: 10.1109/icefeet49149.2020.9187007.

[16] S. S. Salins, A. Hashim, K. A. M. Ansar, M. Hafeez, M. J. Saleem, C. P. Selvan M. "Design and Fabrication of Wind Powered Vehicle," Glob. J. Adv. Eng. Technol., vol. 7, no. 1, 2018.

[17] Y. Gong, Y. Liu, and Z. Tang, "Path tracking of unmanned vehicle based on parameters self-tuning fuzzy control," 2013 IEEE Int. Conf. Cyber Technol. Autom. Control Intell. Syst. IEEE-CYBER 2013, pp. 52–57, 2013, doi: 10.1109/CYBER.2013.6705419.

[18] T. Y. Kim and S. H. LEE, "Combustion and Emission Characteristics of Wood Pyrolysis Oil-Butanol Blended Fuels in a Di Diesel Engine," International Journal of Automotive Technology, vol. 13, no. 2, pp. 293–300, 2012, doi: 10.1007/s12239.

[19] U. H. Rathod, V. Kulkarni, and U. K. Saha, "On the application of machine learning in savonius wind turbine technology: An estimation of turbine performance using artificial neural network and genetic expression programming," J. Energy Resour. Technol. Trans. ASME, vol. 144, no. 6, pp. 1–16, 2022, doi: 10.1115/1.4051736.

[20] Z. Bitar, S. Al Jabi, and I. Khamis, "Modeling and simulation of series DC motors in electric car," Energy Procedia, vol. 50, pp. 460–470, 2014, doi: 10.1016/j.egypro.2014.06.056.

[21] M. A. Shamseldin, "Optimal Coronavirus Optimization Algorithm Based PID Controller for High Performance Brushless DC Motor," algorithms Artic., vol. 14, p. 17, 2021.

[22] A. Rehman Khan, A. Tamoor Khan, M. Salik, and S. Bakhsh, "An Optimally Configured HP-GRU Model Using Hyperband for the Control of Wall Following Robot," Int. J. Robot. Control Syst., vol. 1, no. 1, pp. 66–74, 2021, doi: 10.31763/ijrcs.v1i1.281.

[23] A. Ouda and A. Mohamed, "Autonomous Fuzzy Heading Control for a Multi-Wheeled Combat Vehicle," Int. J. Robot. Control Syst., vol. 1, no. 1, pp. 90–101, 2021, doi: 10.31763/ijrcs.v1i1.286.

[24] R. Boucetta, W. Abdallah, and S. Bel Hadj Ali, "An Adaptive Control for the Path Tracking of an Active Leg Prosthesis," Int. J. Robot. Control Syst., vol. 1, no. 2, pp. 159–176, 2021, doi: 10.31763/ijrcs.v1i2.350.

[25] X. Wei-hong, C. Li-jia, and Z. Chun-lai, "Review of Aerial Manipulator and its Control," Int. J. Robot. Control Syst., vol. 1, no. 3, pp. 308–325, 2021, doi: 10.31763/ijrcs.v1i3.363.

[26] A. N. Kadjie and E. B. T. Tchuisseu, "A Multifunction Robot Based on the Slider-Crank Mechanism: Dynamics and Optimal Configuration for Energy Harvesting," Int. J. Robot. Control Syst., vol. 1, no. 3, pp. 269–284, 2021.

[27] E. Rahimi khoygani, M. R. Rahimi khoygani, and R. Ghasemi, "Intelligent Observer-Based Controller Design for Nonlinear Type-1 Diabetes Model via Adaptive Neural Network Method," Int. J. Robot. Control Syst., vol. 1, no. 3, pp. 338–354, 2021, doi: 10.31763/ijrcs.v1i3.442.

[28] E. S. Rahayu, A. Ma'arif, and A. Çakan, "Particle Swarm Optimization (PSO) Tuning of PID Control on DC Motor," Int. J. Robot. Control Syst., vol. 2, no. 2, pp. 435–447, 2022.

[29] M. Tahmasebi, M. Gohari, and A. Emami, "An Autonomous Pesticide Sprayer Robot with a Color-based Vision System," Int. J. Robot. Control Syst., vol. 2, no. 1, pp. 115–123, 2022, doi: 10.31763/ijrcs.v2i1.480.

[30] Y. Zahraoui, M. Akherraz, and A. Ma'arif, "A Comparative Study of Nonlinear Control Schemes for Induction Motor Operation Improvement," Int. J. Robot. Control Syst., vol. 2, no. 1, pp. 1–17, 2021, doi: 10.31763/ijrcs.v2i1.521.

[31] A. K. Ali and M. M. Mahmoud, "Methodologies and Applications of Artificial Intelligence in Systems Engineering," Int. J. Robot. Control Syst., vol. 2, no. 1, pp. 201–229, 2022, doi: 10.31763/ijrcs.v2i1.532.

[32] H. A. Hefny and S. S. Azab, "Chaotic particle swarm optimization," INFOS2010 - 2010 7th Int. Conf. Informatics Syst., vol. 1, no. 4, pp. 523–533, 2010.

[33] A. W. L. Yao and H. C. Chen, "An Intelligent Color Image Recognition and Mobile Control System for Robotic Arm," Int. J. Robot. Control Syst., vol. 2, no. 1, pp. 97–104, 2022, doi: 10.31763/ijrcs.v2i1.557.

[34] M. H. H. Rosman et al., "Real-Time Underground Plastic Pipeline Water Leakage Detection and Monitoring System," Int. J. Robot. Control Syst., vol. 2, no. 2, pp. 424–434, 2022.

[35] M. Maaruf, M. S. Mahmoud, A. Ma'arif, "A Survey of Control Methods for Quadrotor UAV," Int. J. Robot. Control Syst., vol. 2, no. 4, pp. 652–664, 2022.

[36] M. S. Mahmoud and A. H. AlRamadhan, "Optimizing the Parameters of Sliding Mode Controllers for Stepper Motor through Simulink Response Optimizer Application," Int. J. Robot. Control Syst., vol. 1, no. 2, pp. 209–225, 2021.

[37] M. I. Faiq Hatta and N. Satya Widodo, "Robot Operating System (ROS) in Quadcopter Flying Robot Using Telemetry System," Int. J. Robot. Control Syst., vol. 1, no. 1, pp. 54–65, 2021, doi: 10.31763/ijrcs.v1i1.247.

[38] D. S. Febriyan and R. Dwi Puriyanto, "Implementation of DC Motor PID Control On Conveyor for Separating Potato Seeds by Weight," Int. J. Robot. Control Syst., vol. 1, no. 1, pp. 15–26, 2021, doi: 10.31763/ijrcs.v1i1.221.

[39] M. H. Iqbal and W. S. Aji, "Wall Following Control System with PID Control and Ultrasonic Sensor for KRAI 2018 Robot," Int. J. Robot. Control Syst., vol. 1, no. 1, pp. 1–14, 2021, doi: 10.31763/ijrcs.v1i1.206.

[40] M. A. Shamseldin et al., "A New Design Identification and Control Based on GA Optimization for an Autonomous Wheelchair," Robotics, vol. 11, no. 5, p. 101, 2022.

[41] L. M. El-Tehewy, M. A. Shamseldin, M. Sallam, and A. M. Abdel Ghany, "A Modified Model Reference Adaptive Control for High-Performance Pantograph Robot Mechanism," Wseas Trans. Appl. Theor. Mech., vol. 16, pp. 193–203, 2021, doi: 10.37394/232011.2021.16.22.

[42] M. A. Shamseldin, "Optimal Covid-19 Based PD/PID Cascaded Tracking Control for Robot Arm driven by BLDC Motor," Wseas Trans. Syst., vol. 20, pp. 217–227, 2021, doi: 10.37394/23202.2021.20.24.

[43] E. Emad, O. Alaa, M. Hossam, M. Ashraf, and M. A. Shamseldin, "Design and Implementation of a Low-Cost Microcontroller-Based an Industrial Delta Robot," Wseas Trans. Comput., vol. 20, pp. 289–300, 2021, doi: 10.37394/23205.2021.20.32.

[44] M. A. Ghany and M. A. Shamseldin, "Sliding Mode Self-Tuned Single Neuron PID Controller for Power System Stabilizer," Wseas Trans. Comput., vol. 20, pp. 309–320, 2021, doi: 10.37394/23205.2021.20.34.

[45] X. Xi, A. Poo, and G. Hong, "Tracking error-based static friction compensation for a bi-axial CNC machine," Precis. Eng., vol. 34, no. 3, pp. 480–488, 2010, doi: 10.1016/j.precisioneng.2009.12.003.

[46] V. Nguyen and C. Lin, "Adaptive PD Networks Tracking Control with Full- State Constraints for Redundant Parallel Manipulators," in IFSA-SCIS 2017, 2017, no. 4, pp. 0–4.

[47] S. Wen, T. Wang, Z. Ma, and X. Li, "Dynamics Modeling and Fuzzy PD Control of Humanoid Arm," in Proceedings of the 36th Chinese Control Conference, 2017, no. 3, pp. 616–621.

[48] A. Bennaoui, S. Saadi, and A. Ameur, "Performance Comparison of MFO and PSO for Optimal Tuning the fractional order fuzzy PID Controller for A DC-DC Boost Converter," 2020 Int. Conf. Electr. Eng. ICEE 2020, 2020, doi: 10.1109/ICEE49691.2020.9249778.

[49] M. A. Abdel Ghany, M. A. Shamseldin, and A. M. Abdel Ghany, "A novel fuzzy self tuning technique of single neuron PID controller for brushless DC motor," Int. J. Power Electron. Drive Syst., vol. 8, no. 4, 2017, doi: 10.11591/ijpeds.v8i4.pp1705-1713.

[50] J. C. Shen and C. S. Ye, "Precision Fuzzy Sliding-mode Tracking Control with DNLRX Model Based Friction," in 2018 SICE International Symposium on Control Systems (SICE ISCS), pp. 27-32 2018.

[51] A. A. El-samahy and M. A. Shamseldin, "Brushless DC motor tracking control using self-tuning fuzzy PID control and model reference adaptive control," Ain Shams Eng. J., 2016, doi: 10.1016/j.asej.2016.02.004.

[52] A. Franchi and A. Mallet, "Adaptive Closed-loop Speed Control of BLDC Motors with Applications to Multi-rotor Aerial Vehicles," in 2017 IEEE International Conference on Robotics and Automation (ICRA) Singapore., 2017, no. 978, pp. 5203–5208.

[53] W. Netto, R. Lakhani, and S. M. Sundaram, "Design and performance comparison of different adaptive control schemes for pitch angle control in a Twin-Rotor-MIMO-System," Int. J. Electr. Comput. Eng., vol. 9, no. 5, pp. 4114–4129, 2019, doi: 10.11591/ijece.v9i5.pp4114-4129.

[54] L. Yang, Z. Q. Zhu, B. Shuang, and H. Bin, "Adaptive Threshold Correction Strategy for Sensorless High-Speed Brushless DC Drives Considering Zero-Crossing-Point Deviation," IEEE Trans. Ind. Electron., vol. 67, no. 7, pp. 5246–5257, 2020, doi: 10.1109/TIE.2019.2931501.

[55] P. Swarnkar, "Effect of Adaptation Gain in Model Reference Adaptive Controlled Second Order System," Eng. Technol. Appl. Sci. Res., vol. 1, no. 3, pp. 70–75, 2011.

[56] R. Madiouni, "Robust PID Controller Design based on Multi-Objective Particle Swarm Optimization Approach," in ICEMIS2017, 2017, pp. 1–7.

[57] C. Sun, G. Gong, F. Wang, H. Yang, and X. Ouyang, "Single Neuron Adaptive PID Control for Hydro-viscous Drive Clutch," in 12th IEEE/ASME International Conference on Mechatronic and Embedded Systems and Applications (MESA), 2016, no. 3, pp. 3–6.

[58] A. M. Khalid, H. M. Hamza, S. Mirjalili, and K. M. Hosny, " BCOVIDOA: A Novel Binary Coronavirus Disease Optimization Algorithm for Feature Selection," Knowledge-Based Systems, vol. 248, 2022.

[59] F. Martínez-Álvarez et al., "Coronavirus Optimization Algorithm: A Bioinspired Metaheuristic Based on the COVID-19 Propagation

Model," Big Data, vol. 8, no. 4, pp. 308–322, 2020, doi: 10.1089/big.2020.0051.

[60] S. A. Alanazi, M. M. Kamruzzaman, M. Alruwaili, N. Alshammari, S. A. Alqahtani, and A. Karime, "Measuring and Preventing COVID-19 Using the SIR Model and Machine Learning in Smart Health Care," J. Healthc. Eng., vol. 2020, 2020, doi: 10.1155/2020/8857346.